nPSF: PSF Fitting Software for Trans-Neptunian Objects

William Giforos

A senior thesis submitted to the faculty of
Brigham Young University
in partial fulfillment of the requirements for the degree of

Bachelor of Science

Darin Ragozzine, Advisor

Department of Physics and Astronomy

Brigham Young University

ABSTRACT

nPSF: PSF Fitting Software for Trans-Neptunian Objects

William Giforos
Department of Physics and Astronomy, BYU
Bachelor of Science

Orbital systems of two or more Trans-Neptunian Objects (TNOs) are valuable for investigating formation processes of the early Solar System. Because TNOs exist below the diffraction limit of current telescopes, they are rendered as point spread functions (PSFs) in observational images. To correctly understand the orbital dynamics of TNO systems, the PSFs must be modeled according to telescope, camera, and observational parameters. These models can then be fit to images to produce the precise relative astrometry that is needed to fit the orbits. The software package nPSF was designed to fit modeled PSFs to images containing an $n$ number of PSFs using Bayesian parameter inference methods, specifically the Markov Chain Monte Carlo process. The relative astrometry of the system can then be derived from the posterior distribution. We test the capabilities of nPSF by fitting images of 2PSF Trans-Neptunian Binaries and comparing our results to the published astrometry for those systems. We show that nPSF produces good astrometry in the tested systems. Additionally, we apply nPSF to the search of a tertiary object in various potential hierarchical triple systems. The results produced by nPSF do not indicate the detection of a third component in these systems.

ACKNOWLEDGMENTS

# Contents

# List of Figures

# List of Tables

# Chapter 1

# Introduction

Over the years, our understanding of the Solar System, Galaxies, and the Universe in general has grown exponentially with the improvement of telescopes and cameras. Billions of people enjoy the basic ability to Google awe inspiring images of planets, nebulae, and multitudes of galaxies. Despite the astounding detail in these images, there are numerous astronomical objects that are incapable of being imaged at such a detailed level. One such case includes Trans-Neptunian Objects (TNOs), which are icy bodies that exist just beyond the orbit of Neptune in the Kuiper Belt. The comparatively small size of TNOs renders them below the diffraction limit of the Hubble Space Telescope (HST), which limit determines the information that can be resolved into an image. Anything below this limit can only be interpreted as a source of light with negligible dimensions, also known as a point source.

## 1.1   TNOs are Information Rich Systems

The point source problem makes studying the nature of TNOs rather difficult, thereby motivating us to improve upon existing methods. This improvement is necessary because the position of TNOs in the Solar System makes them compelling sources of information. Being the furthest objects from

the Sun that are bound to our Solar System, TNOs are primordial in nature because they are far from the gravitational effects of planets and have relatively unchanged compositions from solar heating. Given these characteristics, TNOs are good markers for conditions that existed just after the formation of the solar system, thereby retaining the possibility of providing rich information regarding planet formation processes.

Of the thousands of TNOs in the Kuiper Belt, there are 86 known TNOs that are accompanied by one or more moons (Noll et al. 2020). Systems of two TNOs gravitationally bound together are called Trans-Neptunian Binaries (TNBs), leading us to dub systems with three or more objects as Trans-Neptunian Multiples (TNMs). These binaries/multiples are significant to our research because a popular planetary formation theory known as the streaming instability favors the formation of multiple bodies at a time (Nesvorny et al. 2019). This would suggest the existence of many TNOs grouped together in systems of two or more bodies. To better connect the dots, we need to gain more information about these binary/multiple systems. The most efficient way to get that information is through orbit fitting.

## 1.2   Relative Astrometry

TNBs have a binary orbital period of anywhere between a few days to a few thousand. This indicates that their orbits can't be solved from observations made in a single night. Even so, information from many images taken at different observational dates can be used to fit an orbit to the data. The data required to do this is known as relative astrometry and is essentially a data set of the position of the objects relative to each other within a dynamical orbit. For TNO systems, the objects are generally well enough separated to be seen as distinguishable point sources in an image, making it possible to get a general sense of the astrometry. However, getting a realistic fit to the orbit depends on our relative astrometry being as precise as possible. This becomes rather difficult given the response of

astronomy imaging equipment to point source detection.

## 1.3   Point Spread Functions

When a focused optical imaging system captures the image of a point source, the shape and size of the image is described by a point spread function (PSF). This entails the spreading of the point source across multiple pixels on the detector interface of the imaging system. The result is the image of a smeary blob in place of a well defined object . These PSFs make it impossible to determine the exact position of the point source by examining the image manually. To effectively determine the correct position, knowledge of the imaging system response to point source detection is necessary. Because PSFs are caused by the diffraction of light onto a detector, the response is unique to the telescope and camera in use, as well as the observing circumstances at the time the images were taken. These unique factors mean that a new PSF model must be generated for any given set of data. To do this efficiently, we employ TIM (Telescope Imaging Modeling) PSF modeling software, also known as Tiny Tim (Krist et al. 2011). However, once the PSF model has been constructed, it must be fit to the HST image as carefully as possible to provide accurate positional information. To accomplish this task, we developed the new software package nPSF.

## 1.4   The nPSF Software Package

The nPSF software is designed to fit multiple PSFs generated by Tiny Tim to HST images of TNBs taken with the Wide Field Camera 3 (WFC3). It performs this task utilizing Bayesian Statistics and the Markov Chain Monte Carlo (MCMC) method to randomly sample possible fits. Fitting results are returned as a probability distribution of the sampled fits. Positional parameters $x$ and $y$ are explored in these fits, as well as brightness (height $h$) and focus ($f$) parameters. Determining the positional arguments provides us with the relative astrometry we are looking for. This is accomplished by

nPSF through derivations involving the median of the returned probability distribution. By running nPSF on many images of the same TNB, sufficient astrometry can be derived to solve the orbit of the system via a separate software program called MultiMoon, which uses similar statistical processes to fit an orbit to the data and is briefly discussed in this paper.

We developed nPSF in Python due to the accessibility of supporting packages such as astropy and emcee. Astropy provides useful tools for performing relative astrometry analysis on parameter results returned by nPSF (The Astropy Collaboration, et al. 2018). Emcee is a python implementation of MCMC (Foreman-Mackey et al. 2013). Python is also more readily accessible to students newer to coding than more rigorous programming languages. Accessibility is our priority with nPSF because it is geared towards students relatively new to research that are looking to contribute in meaningful ways.

To ascertain its reliability as a PSF fitting software, nPSF is still undergoing numerous improvements. Analyses performed on several TNBs with known astrometry have returned values fairly consistent with published results. Accuracy testing analysis has not yet been attempted for systems with 3 PSFs, and the capability for nPSF to tackle systems of 4 or more PSFs remains to be implemented. However, nPSF was applied to several TNB systems suspected of containing an undetected third body, also known as hierarchical triples. Fits of several images of these systems returned no detection of a third component. We plan to more thoroughly test nPSF's capabilities against published values of TNO systems with two to three objects to ensure its usefulness and accuracy as a PSF fitting tool.

This code was originally developed by students in the Advanced Observational Astronomy course at BYU, with the bulk of the code written by BYU graduate student Benjamin Proudfoot. Since its initial conception, I have implemented updates and changes to further progress the vision of nPSF and its compatibility with MultiMoon.

# 1.5 Paper Overview

The purpose of this document is to outline the modeling processes at the core of nPSF. The theory involved, including Bayesian parameter inference and MCMC, is discussed in Section 2.1. This is followed by an outline of nPSF's functionality in Section 2.2 and its application in Section 2.3. The results of this application are laid out in Chapter 3 and are split between our testing of 2PSFs and our 3PSF search for a 3rd component in potential hierarchical triple systems. Discussion of our results concludes the document in Section 3.3.

# Chapter 2

# Methods

To produce useful data from HST images of TNOs, we attempt to fit PSF models to our data. This procedure includes the estimating of certain values intrinsic to the fitting process that cannot be predetermined by the model. These intrinsic values are called free parameters and their theoretical or experimental estimation is a statistical process known as parameter inference. The free parameters are important for PSF fitting because it defines the placement of the model to match the data.

## 2.1 Theoretical Approach

The free parameters involved in our PSF fitting include the $x$ and $y$ position values and the point source pixel values, which is determined by how bright the point source appears and is referred to as height $h$ in nPSF. Our final free parameter of our model is the focus $f$ of the HST telescope. The focus changes as the telescope travels through its orbit due to thermal effects altering the position of the secondary mirror (Krist & Hook 2004). Because the telescope's focus at the time the image was taken affects the point source PSF, we account for this change in focus by generating multiple PSF models with Tiny Tim over a range of focus values. This way, the focus parameter space can also be explored in the fitting process.

### 2.1.1   Bayesian Statistics

When dealing with parameter inference, it is important to be able to understand both the best fit solution and its accompanying uncertainties. To accomplish this, we use an approach that involves Bayesian statistics. We determined Bayesian inference to be an appropriate approach because its posterior solution produces a probability distribution of every parameter given in our data. A probability distribution (or density) function (PDF) is a statistical function that describes how likely it is for a random variable to take on various probable values. Bayesian inference is motivated by Bayes' Law, given here:

$$p(\Theta|D) = \frac{p(D|\Theta)p(\Theta)}{p(D)} \tag{2.1}$$

When applying Bayesian inference, we want to find the joint probability distribution, meaning the probability that our parameter set $\Theta$ occurs given that our data D is true, otherwise represented as $p(\Theta|D)$. However, our data instead informs us of $p(D|\Theta)$, the probability of D occuring given that $\Theta$ is true, which we term the likelihood function. To then find $p(\Theta|D)$, we apply Equ. 2.1, with a prediction $p(\Theta)$ made before knowing our data and our evidence given by $p(D)$, which serves to imperfectly "normalize" the product of the likelihood and the prediction. The solution of this product, $p(\Theta|D)$, is referred to colloquially as the posterior PDF while $p(\Theta)$ is known as the prior PDF (Hogg & Foreman-Mackey 2017).

### 2.1.2   Markov Chain Monte Carlo

We then apply Bayesian parameter inference to our model using the MCMC method. This allows us to explore all parameter space and determine which posterior values are the most accurate measure of the true relative astrometry.

MCMC uses Bayesian statistics to take random samples of the posterior PDF using information from the prior PDF and the likelihood function. This is accomplished by performing a random walk

in the parameter space. This walk is comprised of a user specified number of walkers that each take steps toward a maximum probability value. Each step is a random sample of the posterior PDF whose probability can be interpreted with the likelihood function. Each walker takes one step, then returns that many independent samples of the PDF. MCMC then uses the returned sample likelihoods to guess the best direction to send each walker on their next step, then executes the next step. If a walker takes a step in a direction that increases its likelihood function, it will continue to take steps in that direction. If the new step instead decreases in likelihood, it return to the previous step and computes a new direction to pursue. All the information pertaining to each step taken by the walkers is saved in a chain that is perpetuated until the run terminates (Foreman-Mackey et al. 2013).

Using many walkers together to sample the posterior PDF as described above is known as an ensemble sampler, because the group of walkers maintained by MCMC are treated as a whole rather than individually. nPSF uses an affine invariant ensemble sampler software package called emcee. Affine invariant means that linear transformations don't alter the efficiency of the sampler. This is important because it allows us to apply an affine transformation to turn hard sampling problems into easier ones (Foreman-Mackey et al. 2013).

When using an ensemble sampler to run MCMC, it is important to try and initialize the ensemble walkers in a typical or good position in the posterior PDF. However, doing so is not always trivial, and so a burn-in phase is implemented in the procedure. The burn-in period constitutes exploration of the posterior PDF that is later discarded from the chain. This allows for the ensemble sampler to avoid the non-typical posterior PDF regime results when performing inferences on the sampled distribution. That way, only good sampled values contribute to the posterior analysis (Hogg & Foreman-Mackey 2017).

Another important step is to deal with multi-modal posterior PDFs by using clustering. Multi-modal posterior PDFs are posteriors where there are multiple "peaks," such as can be found in a

mountain range. Obviously the most probable answer is the highest peak, but it can be difficult for walkers to leave a lower peak once they have reached it. To deal with this problem, nPSF employs a clustering algorithm that analyzes the relative "positions" of the walkers and then redeposits walkers trapped in lower peak concentrations with the concentration of walkers exploring the highest peak. This algorithm is sufficient to overcome most multi-modal issues.

The posterior PDF can be thought of being well sampled once an appropriate convergence to a general value is reached. Absolute convergence is impossible due to the discrete optimization problem, so being able to judge convergence is key in our approach. To do this, we use the chi-by-eye method of examining the posterior plots generated by nPSF and determining empirically whether the run has adequately converged or not. With nPSF, this approach is fairly reliable and sufficient for our purposes.

## 2.2   Functionality

The nPSF software requires the input of various parameter values to initiate and perform efficiently. These values can be entered into a specific text file template prepared for this purpose. This file provides nPSF programs with paths to the information stored in the data and results directories. Once the appropriate information has been recorded in this text file, nPSF can then extract that information to perform the run. Parameter starting guesses are also included alongside this file to provide nPSF with a good starting point to begin the MCMC process.

Tiny Tim takes a variety of parameters as inputs to correctly determine the type of PSF found in the HST image being analyzed. These include the detector, chip, psf position, filter name, spectral type, PSF size, and the focus value. Many of these values can be read in directly from the image header. From this information, an array of model PSFs are generated, with the only difference between models being an incremental increase in focus values within the range of possible focus

values suggested by the user.

### 2.2.1  Modeling Processes

HST images of TNBs generally contain many different bright sources that could confuse the PSF fitting process. These include background stars and cosmic rays. Cosmic rays are high energy particles moving through space, and they frequently appear as abnormally bright spots on the CCD camera, termed hot pixels. These hot pixels don't resemble PSFs and can be cleaned using ccdproc, an Astropy image reduction package. Once the cosmic rays have been removed from the image, we take a subsample of the image to avoid dealing with the many PSFs introduced by the background stars. This subsample, called a stamp, is anything larger than a 60 x 60 pixel square centered about the primary TNO. The specific stamp size is provided by the user, as well as a left corner position where the stamp begins.

### 2.2.2  Important Outputs

To generate useful output, a variety of analyses are performed on the returned posterior values. Upon terminating, nPSF returns the chain of each attempted *x*, *y*, and height values for each PSF, with a logarithmic likelihood value describing each set of parameters. Focus values are also included in the chain. The chain of values is then used to derive additional parameters for each step of the chain. These include $\Delta$RA, $\Delta$dec, difference in magnitude ($\Delta$mag), separation distance (sep), position angle or the angle from north (pa), $\Delta$x, and $\Delta$y. Each derived parameter is then grafted into the chain so that analytical outputs can be produced easily.

We then plot the parameters vs. each step's respective likelihood value (previously calculated by nPSF) as a series of graphs. These plots help the user to visualize the best fit values for each parameter and determine whether the posterior distribution was sufficiently sampled in the run. Fig. 2.1 is an example of the likelihood plots, showing position x1 vs. the log likelihood (x1 being

**(a)** Well converged          **(b)** Not converged
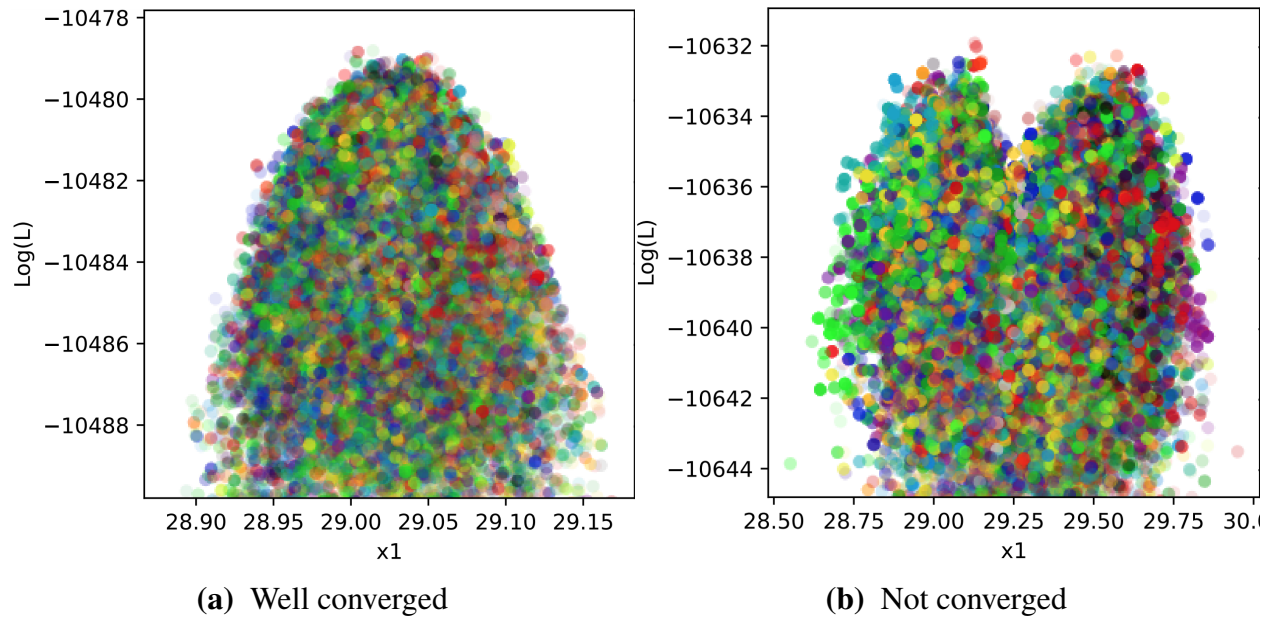
**Figure 2.1** Likelihood plots representing the position x of the primary TNO vs. the log likelihood value of each projected value. Plot **(a)** shows a run that has good convergence while plot **(b)** did not converge.

the x position of the primary TNO). The smooth round peak shown in plot **(a)** of Fig. 2.1 indicates to the user that the PDF was well sampled and that good convergence was reached. The user can also observe the walker plots generated for each parameter if further knowledge of the run's convergence is necessary, as seen in Fig. 2.2. Each color represents a different walker and the path they took to come to their final value at the end of the run. It is fairly simple to see that if the walkers all clustered into a general value by the end of the plot, the run achieved good convergence. If the walkers have instead ended in many different values, convergence was not achieved for the run.

To compress the run's posterior distribution into a useful data set, nPSF then computes the median value of each parameter, along with standard deviations of $\sigma$, $2\sigma$, and $3\sigma$ values. The mean is also computed, but without standard deviations. These summary results are then printed along with the best fit values (value with the highest likelihood) of each parameter in a single file. Additionally, this process is also done for the latitude and longitude values of each object, which

**(a)** Well converged        **(b)** Not converged
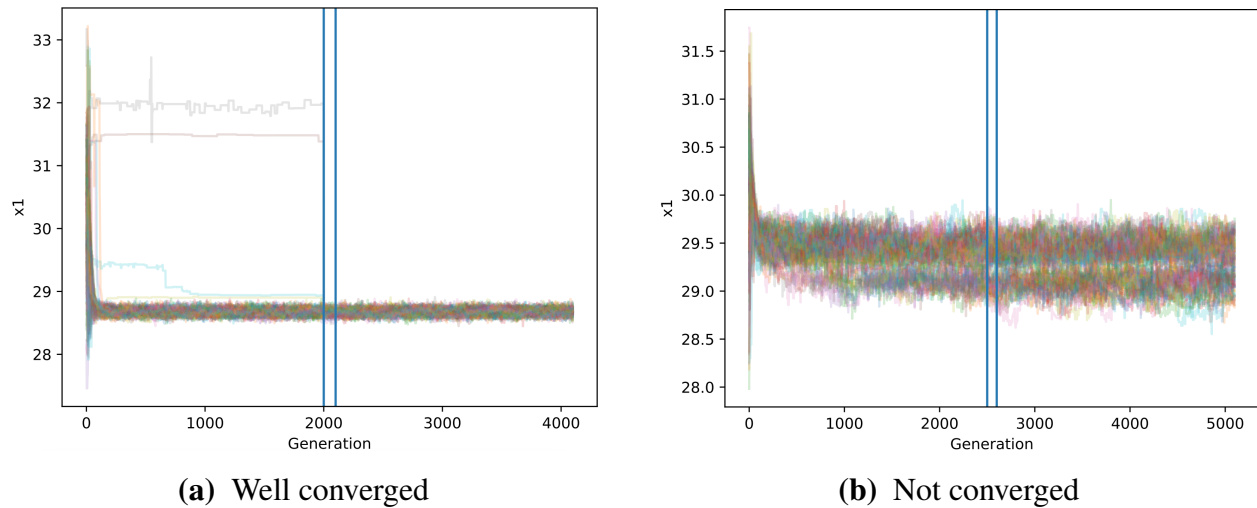
**Figure 2.2** Walker plots showing the convergence of the MCMC walkers. Each walker and its path are represented by different colors. In plot **(a)** we see that the walkers converge after being adjusted by the clustering algorithm once they hit 2000 steps. Plot **(b)** shows the walkers split between two likely values, rendering the clustering algorithm incapable of redirecting misguided walkers to a concrete majority.

have been derived from the ΔRA and Δdec values. These are included in the summary results file, but the median and errors of these values are also printed in a separate file designed specifically in the format of MultiMoon astrometry input, which is another important software our team developed. (More on MultiMoon in Section 2.3.1)

## 2.3   Application

We tested nPSF on 6 different TNB systems. Several images of each pair were run in nPSF and the posterior values were then compared to previously published values for the difference in right ascension and declination between the primary and secondary TNOs, otherwise referred to as ΔRA and Δdec. The results of these tests are surmised and analyzed in Section 3.1.
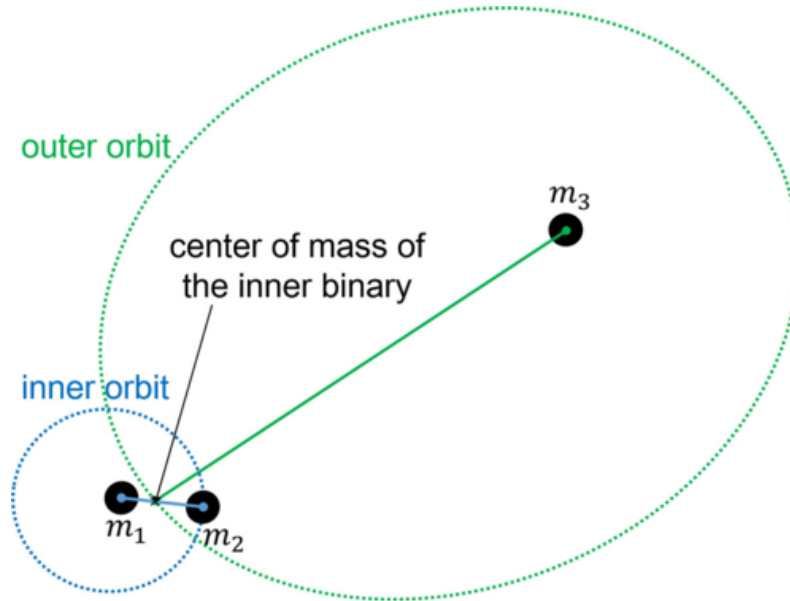
**Figure 2.3** FIG. 1 in Gravitational Waves from Hierarchical Triple Systems with Kozai-Lidov Oscillation, DOI: 10.1103/PhysRevD.101.104053 (Gupta et al. 2020). A hierarchical triple is a system composed of stable inner and outer orbits. The inner mass, $m2$ orbits the primary object $m1$ while the outer mass $m3$ orbits the center of mass of the inner binary.

### 2.3.1  3-body applications

MultiMoon is another Bayesian parameter inference engine designed by our team to fit orbits to TNMs. It uses positional astrometry, such as nPSF output, on as many observed dates as possible to accomplish this. MultiMoon also fits and derives additional orbital parameters that nPSf is incapable of calculating. One such parameter is the oblateness ($J_2$) of the primary object in the system. This parameter is important for describing the physical properties of the primary TNO.

Several of the TNB orbits our team fit in MultiMoon returned $J_2$ values that were physically improbable for an individual TNO. This led us to infer that these systems could possibly have a small 3rd object hidden within the PSF of the primary. Such systems where the primary object has a close companion is known as a hierarchical triple (see Fig. 2.3 (Gupta et al. 2020)). However, the size and proximity of an inner orbit companion can be difficult to detect next to the brightness of the primary object. Indeed, these systems that exhibited high $J_2$ values are currently identified as

binaries, nothing more. These systems include Teharonhiawako & Sawiskera, 2005 EO304, and 2006 BR284. We decided to perform 3PSF fits on each system using nPSF to see if we could detect the predicted tertiary component in existing HST images. The results and analysis of this search are reported in Section 3.2.

# Chapter 3

# Results

Comparing the results of the 2PSF fits we performed with nPSF to previously published astrometry will help us ensure the accuracy of this fitting software. In Section 3.1, we compare our fits to the published astrometry found online at Lowell Observatory Orbit Status of Known Binary TNOs. Additionally, we present our results exploring two of the three potential hierarchical triple systems in Section 3.2. Because we are searching for an undetected third body, we primarily focused on 3PSF fits for the systems. Sections 3.3 summarizes our results and discusses their implications for further development of nPSF.

## 3.1  Testing Results (2PSFs)

We ran 2PSF fits on the TNBs 2001 QC298, Varda-Ilmarë, 1999 RT214, Manwë-Thorondor, Ceto-Phorcys, and Gonggong-Xiangliu. The quantity of objects analyzed here helps to ensure the consistency of results and the ability of nPSF to tackle different image situations, such as visible objects that are very distinguished from each other versus objects that are barely distinguishable. Four images were analyzed on each observation date for TNBs 2001 QC298, Varda-Ilmarë, Ceto-Phorcys, and Gonggong-Xiangliu. TNBs 1999 RT214 and Manwë-Thorondor both had 8 images

Table 3.1.    Relative Astrometry: nPSF vs. Grundy

| Julian Date | Date | Filter | (nPSF - Grundy)/$\sigma$_Grundy | | Grundy | |
| | | | $\Delta$RA | $\Delta$dec | $\Delta$x | $\Delta$y |
| | | | ($\Delta\sigma$) | ($\Delta\sigma$) | (arcsec) | (arcsec) |
| (612239) 2001 QC298 | | | | | | |
| 2455472.8 | 2010/10/03 | F606W/F814W | 0.40645 | -0.70038 | $0.03971 \pm 0.0051$ | $0.14506 \pm 0.00294$ |
| (174567) Varda-Ilmarë | | | | | | |
| 2455466 | 2010/09/27 | F606W | -0.15434 | -0.42335 | $-0.00562 \pm 0.00467$ | $0.13799 \pm 0.00172$ |
| 2455751 | 2011/07/09 | F606W | -0.15527 | -0.016594 | $0.08235 \pm 0.00858$ | $-0.11167 \pm 0.00413$ |
| (523983) 1999 RT214 | | | | | | |
| | 2014/10/05 | F606W/F814W | -0.00514 | 0.45993 | $-0.0449 \pm 0.00141$ | $-0.07114 \pm 0.00302$ |
| (385446) Manwë-Thorondor | | | | | | |
| | 2013/11/20 | F606W/F438W | 1.25105 | 0.41284 | $0.19644 \pm 0.00272$ | $-0.1057 \pm 0.00387$ |
| (65489) Ceto-Phorcys | | | | | | |
| | 2010/07/03 | F606W/F814W | 1.61976 | -0.69582 | $-0.01605 \pm 0.00162$ | $-0.06501 \pm 0.00361$ |

total for their individual observation dates. Each image was taken by HST with the WFC3-UVIS
camera, which is in the visible spectrum. In Table 3.1 we report a summary of our results, which are
calculated by taking the difference between the median $\Delta$RA and $\Delta$dec astrometry values returned by
nPSF and the same parameters published at the Lowell Observatory webpage mentioned above. This
page is maintained by Will Grundy, who used the same images we did to solve for the astrometry
on each observation date. This difference is then divided by the standard deviation error found
by Grundy to tell us whether our results are within one standard deviation of Grundy's values or
not. Table 3.1 shows that our results are indeed within   1-2 $\sigma$ of Grundy's answers. These results
indicate that astrometry produced by nPSF is about as accurate as the accepted astrometry for these
TNBs.

It should be noted that results for Gonggong-Xiangliu cannot be found in Table 3.1. This was
due to the fact that Xiangliu proved to be too faint in brightness to pick up next to Gonggong, which
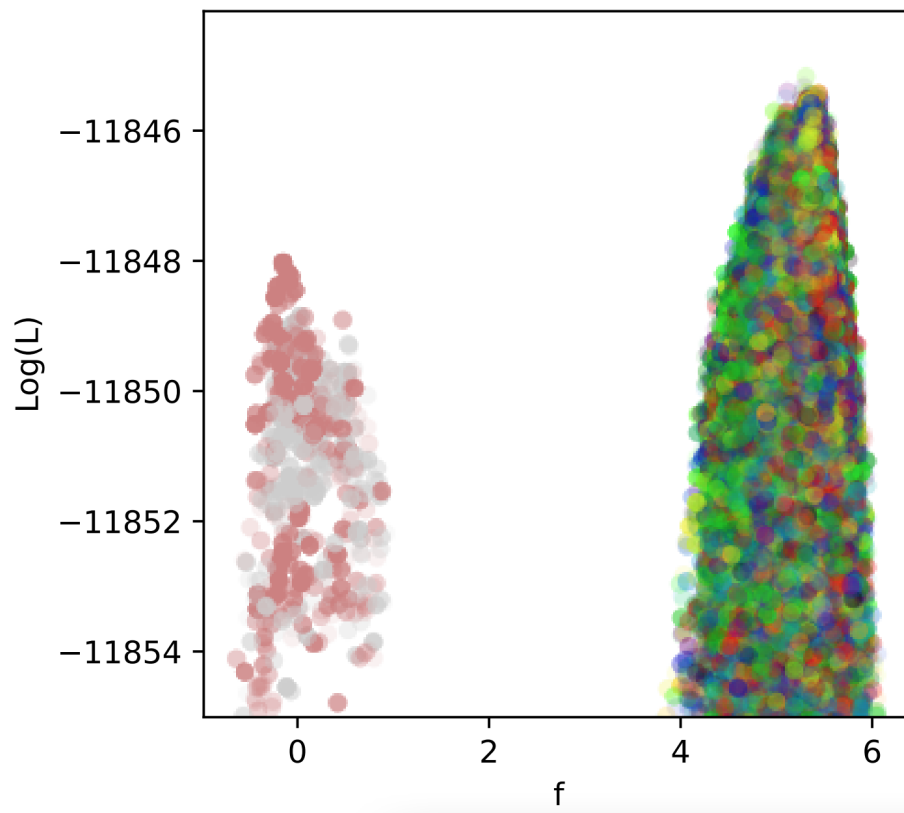
**Figure 3.1** Varda-Ilmarë image ibjb04ovq_flc.fit shows incomplete convergence for the focus parameter of the fit. However, an obvious preference is shown at a value of 5 and the other parameters returned astrometry values similar to Grundy.

itself is much larger and brighter than Xiangliu. We attempted to pinpoint Xiangliu on three different nights of data, but after running nPSF on eight different images, only one of them returned a value somewhat close to published astrometry for Gonggong-Xiangliu. However, Xiangliu was discovered about nine years after the discovery of Gonggong, so the difficulty of solving its astrometry is understandable.

We also address that the results presented for 2001 QC298 are based off an assumed mistake in the publication of the ΔRA error for the observation date 2010/10/03. The Lowell Observatory webpage reports an error of 0.00051 for the ΔRA position (labeled Δx), which causes our results to differ from Grundy's by 4.06455 standard deviations. This is the only astrometry value we found to differ from the published astrometry by such a large amount, making the difference hard to believe. We find that if the published error of 0.00051 is assumed to be a typo, with the correct error being 0.0051, then our result differs from Grundy's by only 0.40645 standard deviations. This is much closer to the trend of our other results, and so this explanation for the apparent discrepancy appears to be highly plausible.

We found the PSF fits represented in Table 3.1 to be well explored and sufficiently converged, with the exception of the image ibjb04ovq_flc.fit of Varda-Ilmarë on the observation date 2011/07/09. Subsequent runs of this image further improved the fit, however, our final run still contained a discrepancy in the focus parameter, as can be seen in Fig. 3.1. Due to the obvious preference of a focus value of 5 and the consistency of finding ΔRA and Δdec values that agree with Grundy's results, we deemed this fit to be adequately explored. It should also be mentioned that 2 of the 4 images taken on this observation date had an exposure time of 0, thereby rendering the images useless. The results given in Table 3.1 on 2011/07/09 are the average of the 2 good images.

Table 3.2.   Hierarchical Triple Search

| Julian Date | Date | Telescope/Instrument | Filter | # Images |
|---|---|---|---|---|
| (525462) 2005 EO304 | | | | |
| 2458866.497 | 2020/01/17 | HST/WFC3-UVIS | F606W | 2 |
| | | | F814W | 4 |
| (88611) Teharonhiawako-Sawiskera | | | | |
| 2455516.284 | 2010/11/15 | HST/WFC3-UVIS | F606W | 2 |
| | | | F814W | 2 |
| 2455483.830 | 2010/10/14 | HST/WFC3-UVIS | F606W | 2 |
| | | | F814W | 1 |

## 3.2   Hierarchical Triple Results (3PSFs)

We ran nPSF on 2 (Teharonhiawako & Sawiskera, 2005 EO304) of the 3 systems that showed significant evidence for hierarchical triples. The third system (2006 BR284) did not have flc.fits file images, which are the necessary files nPSF needs to run accurate analysis.

Table 3.2 shows a summary of the images that were analyzed for each system. Our 3PSF fits for each image returned a variety of results. For 2005 EO304, only one image produced results to suggest that a 3PSF fit could be correct. However, these fits also showed that the lack of a 3rd PSF in the image was almost equally as likely. The other 2005 EO305 images did not show any detection of a 3rd PSF in their runs.

The Teharonhiawako-Sawiskera fits showed more detections of a 3rd PSF in the images, but the 3rd component was never detected in the same place for a given observation date. This obviously indicated that such detections were not plausible. To try to increase nPSF's sensitivity to faint objects in an image, we tried to lower the limit that keeps nPSF from detecting the background noise of the image. Doing so led to abnormal run results and detections of residual cosmic ray influences

that had not been fully cleaned from the images. We subsequently abandoned this technique and concluded that nPSF could not detect any 3rd component to the Teharonhiawako-Sawiskera system.

Our unsuccessful 3PSF fits led us to want to better understand whether detecting a third object in these systems with nPSF could even be feasible. To do this, I used a plotting script Benjamin Proudfoot designed to demonstrate the relationship between semimajor axis and the mass ratio of the primary and 3rd objects. Taking this script, I added limits to the plot to indicate where HST resolution could have resolved the 3rd body in its images. The results of this approach are found in Fig. 3.2, which plots the separation between the tertiary and primary objects (known as semimajor axis $a$) against the mass ratio of the tertiary over the primary ($\frac{M_{in}}{M_{prim}}$). This relationship is defined in terms of the $J_2$ value as given in Equ. 3.1. The Median $J_2$ is plotted here along with 1,2, and 3 $\sigma$ error limits.

$$J_2 R^2 = \frac{a^2 \frac{M_{in}}{M_{prim}}}{2(1 + \frac{M_{in}}{M_{prim}})^2} \tag{3.1}$$

The dotted lines in the plots represent significant constraints on either the existence or detectability of a 3rd component in each potential TNM system. The radius of the primary object and the periapsis of the secondary object (labeled "Beta" for nameless secondaries) constrain the area in between which the tertiary could exist in a stable hierarchical triple system. To be detectable by HST, the tertiary should be sufficiently separated from the primary as to allow HST to resolve the tertiary into a separate PSF, which is represented by being ∼3 WFC3 pixels away from the primary. Additionally, the approximate detectability limit in the graph represents the minimum size of the tertiary object such that it is sufficiently bright as to be detectable. These dectability constraints define a grey area in the plot where the tertiary object should have been detected in HST images if it truly existed.

The plotted relationship given by Equ. 3.1 in Fig. 3.2 indicates that our predicted tertiary object should fall well within the dectability constraints (shaded in grey). These results directly contradict

**(a)**



**(b)**



**(c)**
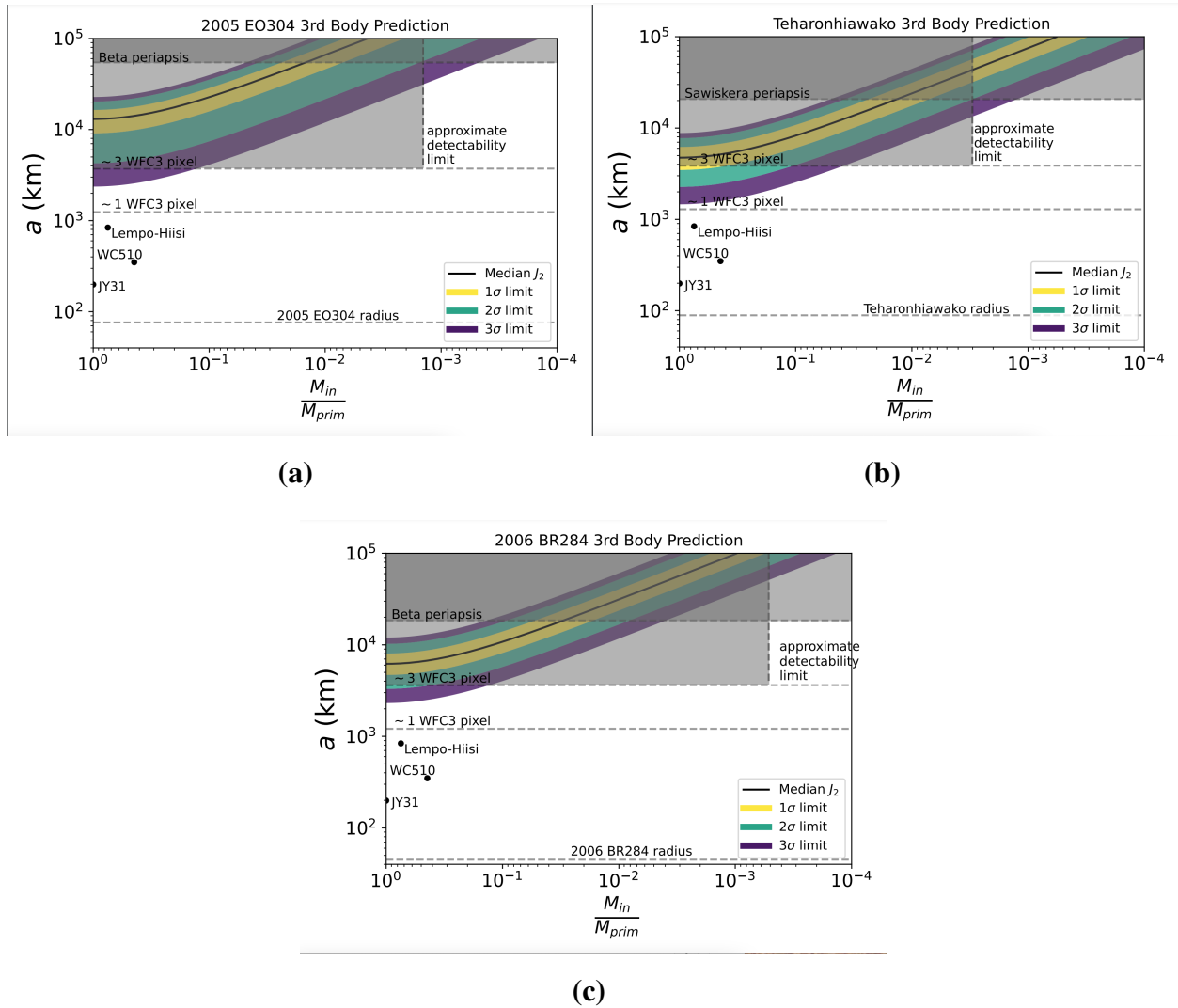
**Figure 3.2** Projected mass ratio ($\frac{M_{in}}{M_{prim}}$) vs. semi-major axis ($a$) values derived from the J2 solutions of each object (see Equ. 3.1). The vertical approximate detectability limit indicates how small the 3rd component could be and still be seen. The 3rd component should also be detectable beyond a separation distance of that HST could resolve into ~3 WFC3 pixels. The 3rd component would cease to be stable at a distance beyond the periapsis of the 2nd component and would no longer be constrained to the system. Our predicted 3rd component falls within the detectability limits outlined here.

our inability to detect a tertiary object in our 3PSF fits of these TNM systems.

## 3.3    Conclusions

The main motivation of nPSF is to provide precise relative astrometry for orbit fitting. We postulated that nPSF has the capabilities to fulfill this function. Upon testing nPSF on TNBs with published astrometry values, we reproduced similar values to Will Grundy's published astrometry for the majority of our results. This shows that nPSF fulfills the requirements we have set forth to be considered sufficiently accurate in its PSF fitting capabilities.

Fig. 3.2 yields the confusing conclusion that if a third object existed in our potential hierarchical triple systems, then HST should have detected them. However, our analysis of the system did not yield sure detections of a third component. One possible explanation is that nPSF is not quite capable of 3PSF fits yet. nPSF has not yet been rigorously tested concerning its 3PSF capabilities, so this is definitely a necessary first step to understanding the issues in our fits. Additionally, it is possible that MultiMoon did not have enough astrometry to produce reliable orbital fits for these 3 systems. Such a case would further support the crucial nature of precise astrometry measurements and the need nPSF fills in our research efforts. Future work will test nPSF's 3PSF fits to ensure its ability to tackle 3-body systems before returning to our analysis of the potential hierarchical triple systems.

# Bibliography

Foreman-Mackey, D., Hogg, D. W., Lang, D., & Goodman, J. 2013, P.A.S.P., 125, 306

Gupta, P., Suzuki, H., Okawa, H., & Maeda, K.-i. 2020, Phys. Rev. D, 101, 104053

Hogg, D. W., & Foreman-Mackey, D. 2017, The Astrophysical Journal Supplement Series, 236

Krist, J., & Hook, R. 2004

Krist, J. E., Hook, R. N., & Stoehr, F. 2011, Proc. SPIE 8127, 8127

Nesvorny, D., Li, R., & Youdin, A. N., et al. 2019, Nat. Astron., 3, 808–812

Noll, K. S., Grundy, W. M., Nesvorný, D., & Thirouin, A. 2020, in The Trans-Neptunian Solar System, ed. D. Prialnik, M. A. Barucci, & L. A. Young (Elsevier), 205–224

The Astropy Collaboration, et al. 2018, A.J., 156, 19

# Index